Development and Commissioning of a Chemiluminescence Imaging System for an Optically-Accessible High-Pressure Generic Swirl Burner

J. Runyon[*, 1], R. Marsh[1], Y. Sevcenco[1], D. Pugh [1], S. Morris[1]

[1]Cardiff University, Wales, United Kingdom

Abstract

A chemiluminescence imaging system has been commissioned at Cardiff University's Gas Turbine Research Centre. OH* and CH* chemiluminescence measurements were initially made on swirl-stabilised methane flames to find the optimal settings of intensifier gate timing, gain, and UV lens f-stop. Measurements with gate widths down to 100 μs have been achieved on methane flames with thermal powers up to 100 kW, pressures up to 3 bara, and global equivalence ratios of 0.6 to 1.2. OH* and CH* chemiluminescence intensities are found to vary with each parameter and yield sufficient spatial information to confirm visual evidence of stable flame operation as well as both lean and rich stability limits. Additionally, the OH*/CH* chemiluminescence intensity ratio is used for evaluation of the local equivalence ratio within the flame. Further OH* and CH* chemiluminescence measurements were made on BOS gas (65% CO, 34% N_2, 1% H_2) flames at comparable conditions to the CH_4 flames to investigate the change in intensities, with marked variation identified between the two fuel blends. In addition to developing measurement capability, image processing and deconvolution techniques have also been integrated into the chemiluminescence system, extending the fundamental combustion research capabilities of the Gas Turbine Research Centre.

Introduction

Non-intrusive optical measurement techniques have been the subject of much research and development over the past few decades in the field of fundamental combustion diagnostics. These techniques provide enhanced flame measurement capability, which results from the undisturbed flow field and non-interaction with the flame front. Among these techniques, chemiluminescence imaging of reactive combustion species (e.g. OH* and CH*) has been shown to provide fundamental measures of flame structure [1, 2], heat release [3, 4], and equivalence ratio [5]. At Cardiff University's Gas Turbine Research Centre (GTRC), a chemiluminescence imaging system has been commissioned for use on the High Pressure Optical Chamber (HPOC), which provides optical access to both axial and radial-tangential planes of the High-Pressure Generic Swirl Burner (HPGSB). The system is based on a CCD camera coupled with a high-speed gated image intensifier and associated optics for wavelength filtering of combustion species chemiluminescence emission, with system timing and image capture controlled via proprietary software. Additional system design considerations include temperature stability of the imaging system, remote access during rig operation, and control of ignition sources due to the proximity of some system electrical components to potential explosive atmospheres.

The study of emission spectra of electronically excited species resulting from chemical processes within a flame has progressed significantly from the early 1950s, when Broida and Gaydon [6] required exposure times of up to 30 minutes on medium quartz spectrographs in order to detect OH* and CH* radicals. Current study of combustion species chemiluminescence is carried out both numerically with the use of advanced chemical kinetics models [7,8] and experimentally, with recent chemiluminescence measurements made at atmospheric pressure on industrial gas turbine combustors from both Alstom (EV-10) [9] and Siemens (SGT-700/800) [10]. The experimental work presented herein aims to demonstrate the use of a modular generic burner capable of pressurised operation and demonstrating new fundamental combustion diagnostic capabilities at the GTRC. Chemiluminescence imaging of the electronically-excited combustion radicals, OH* and CH*, has been performed experimentally across a range of test conditions, with thermal powers up to 100 kW and equivalence ratios of $0.6 < \varphi < 1.2$.

Two separate fuels were used for comparison, with results presented from methane (CH_4)-air flames and a high-CO syngas-air flame representative of basic oxygen steelmaking (BOS) gas, consisting of 65% CO, 34% N_2, and 1% H_2. The dry BOS gas blend used here is unique in both its industrial origin and resulting flame characteristics. Others such as Kutne et al [1] and Sadanandan et al [11] have studied OH* chemiluminescence in hydrogen-rich syngas, but CO-rich syngas has not received as much attention, despite its potential use in the steelworks industry for power and heat generation.

Experimental Setup

The burner (HPGSB) utilised in this study is a medium-scale (< 500 kW) swirl-stabilised premixed generic burner, which was operated at both atmospheric and pressurised conditions up to 3 bara. A quartz confinement tube with an expansion ratio of 3.5:1 was utilised at the exit nozzle for simulation of a gas turbine

[*] Corresponding author: RunyonJP@cardiff.ac.uk

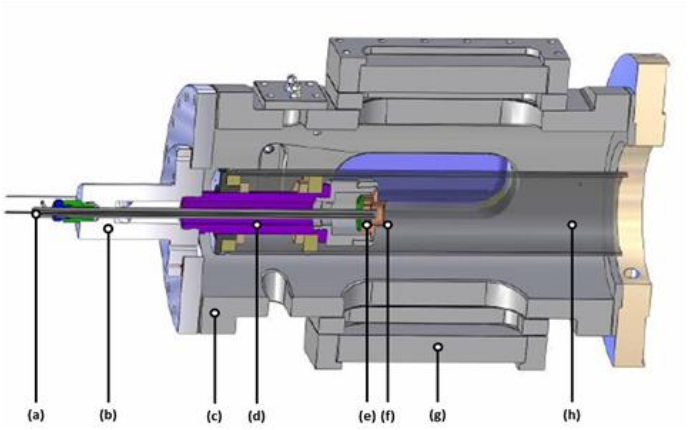

Fig.1 Layout and components of the HPGSB (shown here installed in the HPOC) with igniter (a), inlet plenum (b), HPOC casing (c), premixing chamber (d), slot type radial-tangential swirler (e), exit nozzle (f), quartz window (g), and quartz flame confinement tube (h). Flow from left to right.

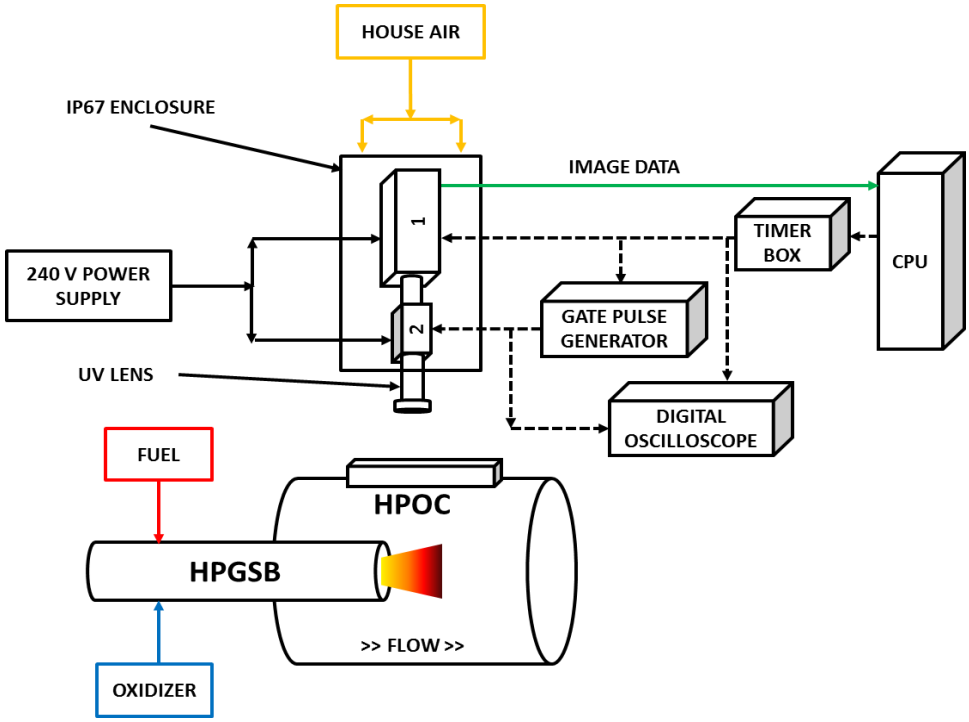

Fig.2 Layout and components of the GTRC's chemiluminescence imaging system, with the HPOC and HPGSB (see Fig.1) shown for reference, where **1** is the CCD camera and **2** is the image intensifier. Both image capture control and utility systems are shown.

combustion chamber and to provide visual access to the burner flame. This burner was installed into the HPOC of the GTRC's High Pressure Combustion Rig (HPCR) for the extent of this work. The configuration and components of the HPGSB can be seen in Fig. 1 as installed in the HPOC. A single axial inlet feeds the gaseous fuel to an outer plenum chamber which uniformly distributes the gas to the slot type radial-tangential swirler. For all experimental cases here, a set geometric swirl number of S_g = 1.04 was used along with a single burner exit nozzle with an inner radius of 20 mm.

Supplies of CH_4 and BOS gas were delivered to the HPGSB by compressed gas cylinders while the air flow was introduced by a compressor capable of delivering up to 50 g/s air flow to the HPGSB mixing plenum. Flow segregation up to the mixing plenum was achieved through the use of isolation and non-return valves on each individual line. The mass flows of air, CH_4, and BOS gas were all monitored and controlled by Micro Motion ELITE Coriolis meters. Pressure in the rig is regulated by the use of a backpressure control valve and

bypass air around the HPGSB.

Existing literature shows that the measurement of chemiluminescence emission from combustion species can be accomplished in a number of different ways, including the use of fibre optics [3], spectrometers [4], novel optical sensors [5,7], and photomultiplier tubes [9,12] However, a number of existing systems [1,2,9-11,13-15] utilise an intensified CCD (ICCD) camera with the appropriate lenses and filters to capture the light emitted from the observed chemical species in the flame. A similar ICCD system was commissioned for this work and can be seen diagrammatically in Fig. 2.

A Dantec Hi Sense Mark II CCD (Model C8484-52-05CP) was used, with 1.38 megapixel resolution (1024 x 1344 pixels) at 16 bits. This allows for a field of view of roughly 60 mm x 80 mm for the arrangement shown. This CCD camera is coupled via a relay lens to a high-speed gated image intensifier (Hamamatsu C9546), a 78 mm UV lens (f/3.8), and a narrow band-pass filter to detect the chemiluminescence emission from the OH* and CH* radicals. The band-pass filter for the OH* radicals is centered at 315 nm ±15 nm while the band-pass filter for the CH* radicals is centered at 430 nm ±15 nm. The ICCD is placed at a 90° angle to the direction of flow, and thus is positioned to capture images through the top window of the HPOC, with the UV lens pointing down into the combustion chamber, focused on the exit nozzle of the HPGSB. Due to its proximity to the HPOC, the ICCD system requires cooling and consideration of potential explosive environments as the optical system is not intrinsically safe. Both design criteria are met by placing the ICCD in an IP67 rated enclosure and purging the enclosure with cool, filtered air to create a positive pressure.

All images from this system are captured via a remote computer via an independent software program, Dantec's DynamicStudio, which also controls timing for the image intensifier gating and camera exposure. The image capture system consists of a trigger timing box (Dantec Timer Box) which provides the trigger signal at a rate of 10 Hz to the CCD camera. The image intensifier requires a gate signal, which must be produced externally by a pulse generator (AMF Venner 728), with the gate pulse synchronised to the trigger pulse sent to the CCD camera. A digital oscilloscope (Tektronix TDS 2024B) is used to monitor the trigger and gate pulses sent to the ICCD system.

Methodology variables

A systematic evaluation of the appropriate equipment settings which impact the intensity of the measured chemiluminescence signal, namely the image intensifier gain (equipment-specific setting), image intensifier gate signal pulse width, and the UV lens f-stop, was performed to identify the ideal settings for OH* and CH* chemiluminescence measurements under the combustion conditions described herein. Previous studies have varied the intensifier gate signal pulse width times for chemiluminescence measurement from 10 µs [10] to 400 µs [16]. To minimise the impact of multiple parameters in the initial experiments, the equipment settings were held constant for all OH* and CH* measurements. Then, a parametric study was initiated with the HPGSB operated at atmospheric pressure with a stable 50 kW methane-air flame at an equivalence ratio of $\varphi = 1$. Each parameter was varied independently, and both OH* and CH* measurements taken to determine the effect of each on the signal intensity.

To measure the effect of image intensifier gain and gate signal pulse widths on the measurements taken, the integral pixel intensity (representing the sum total of all pixel intensity values within an image) was used. Figure 3 shows the effect of image intensifier gain and two intensifier gate signal pulse widths, 1000 µs and 100 µs, on the 2D integral pixel intensity of time-averaged OH* and CH* images. Each measurement is made using an average of 200 images taken at 10 Hz. These images were not background corrected as the intent is to show relative intensities only. The data shows that the gain setting of the intensifier has a greater effect on the measured OH* and CH* signal intensity at higher image intensifier gate times. Also, it appears that the image intensifier gain has a greater effect on the OH* intensity at both pulse widths, particularly above a gain setting of 700.

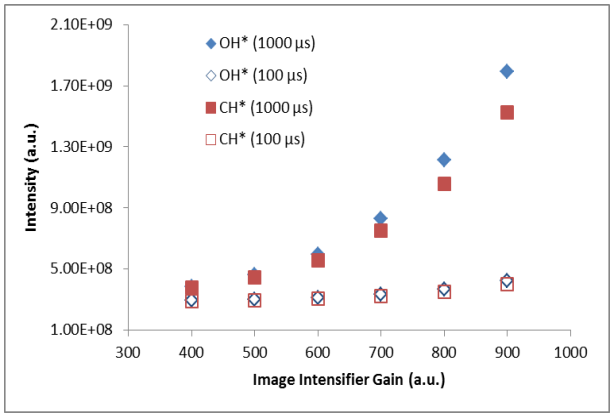

Fig.3 Effect of image intensifier gain and intensifier gate signal pulse width on the integral intensity of the measured OH* (diamond) and CH* (square) signal.

As a result of this analysis, the image intensifier gate pulse width was set to 100 µs to reduce the noise introduced by the intensifier gain, and this value is consistent with that used in [1] for swirl-stabilised flames. To reduce the noise impact of the image intensifier gain further, the intensifier gain is set to 680 (equipment-specific value), while the f-stop of the UV lens set to f/3.8, the lowest available setting resulting in the largest aperture to enhance the measured signal. For all test points, 200 images were captured.

It should be noted that the broadband CO_2* chemiluminescence which has been shown to contribute to both measured OH* and CH* chemiluminescence [4,8,15] has not been accounted for in these or further measurements in this work, as only relative trends are presented.

Image Processing Technique

An evaluation of the literature presented herein indicates that there are not only multiple approaches to the measurement of OH* and CH* chemiluminescence, but also numerous methods utilised for the processing and presentation of chemiluminescence images, with the reporting of time-averaged intensity values [1,12] common along with both background correction [14] and the use of a variety of deconvolution algorithms, including the Abel transformation [10,14,15]. The general method applied here, and described below, involves background removal, temporal averaging, and the use of an Abel inversion for deconvolution of the OH* and CH* chemiluminescence signals.

To determine the appropriate background correction method, the OH* and CH* measurements taken on atmospheric BOS gas flames were evaluated. These images were selected due to the high OH* and CH* signals present, as will be shown in the Results and Discussion section. First, a set of 10 background images were acquired by the ICCD camera with each of the OH* and CH* filters installed individually. These images were then averaged by calculating the mean pixel intensity value across the set of images at each pixel location. Two methods of background correction were investigated, the first requiring subtraction of the averaged background image from each of the 200 individual images and then taking the average of the corrected images while the second method required subtraction of the averaged background image from the ensemble average of the 200 individual images. It was found through an evaluation of mean pixel value and pixel RMS value that both methods produce agreeable results. Thus, the second method is selected as it results in a 65% decrease in image processing time and requires only 1% of the disk space as the first method. Thus, background correction was utilised where possible, however, there were instances, particularly with lean methane-air flames where the CH* chemiluminescence signal was too weak to allow for background correction without complete loss of signal.

As described in [4], chemiluminescence is a line-of-sight technique, meaning that the measured light intensities are integrated, including signal contributions from both in front of and behind the focal plane of the ICCD lens. As such, the resulting image requires deconvolution in order to obtain spatially-resolved information. A MATLAB-based algorithm developed by Killer [17], based on the Abel inversion method described by Pretzler [18], was then utilised to provide spatial representation of the OH* and CH* chemiluminescence measurements. This is a Fourier-based Abel inversion which reconstructs the 2D pixel distribution function through cosine expansions. The selection of the number of cosine expansions utilised in the reconstruction is critical to both filtering effects and computation time. For this work, 5 cosine expansions were used. It was necessary to adapt the algorithm to account for the size of the resulting images (1024 x 1344 pixels) as the algorithm was originally written for analysis of a single row of image pixels. This algorithm assumes that the image to be processed is symmetrical about an axis, processing half an image and then mirroring the image about the axis of symmetry. Given the inherently variable structure of the turbulent swirl flames investigated here, only the time-averaged OH* and CH* chemiluminescence images can be used to ensure symmetry in the axial flow direction. The quartz confinement tube shown in Fig. 1 also provides a boundary for the flame, and the swirler imparts a conical shape on the flame front, thus it is assumed here to be axisymmetric. The algorithm is also optimised for images which have undergone background correction, as it aims to converge on zero pixels values at the image edge parallel to the axis of symmetry. Resulting negative pixel intensity values found after running the algorithm are set to zero.

Figure 4 provides an example of the image processing technique's capability, showing a 50 kW BOS gas-air flame at an equivalence ratio of $\varphi = 0.98$. The resulting image in Fig. 4a is only background corrected and time-averaged, while the image in Fig. 4b is the resulting spatially-resolved OH* chemiluminescence image after Abel inversion. In Fig. 4a, the line-of-sight integration of OH* chemiluminescence from the BOS gas flame provides only an outline of the general conical flame shape, while Fig. 4b gives a more representative shape of the flame, which could be confirmed visually during testing. Note that the pixel intensity scales, representing regions of higher OH radical concentrations, differ between the two images. In this figure (and all chemiluminescence images following), the flow is from top to bottom while the image dimensions are $-32 \text{ mm} < x < 32 \text{ mm}$ (left to right) and $0 < y < 60$ mm (top to bottom).

Results and Discussion

Combustion testing in the HPGSB was first conducted on methane-air flames with thermal powers from 25 to 100 kW, pressures up to 3 bara, and equivalence ratios from $0.62 < \varphi < 1.27$. Both OH* and CH* measurements were taken at each test condition by replacing the band-pass filter on the end of the UV lens (see Fig. 2). OH* chemiluminescence measurements taken on CH_4-air flames at two pressures can be seen in Fig. 5. Figure 5a is a 50 kW atmospheric methane-air flame at an equivalence ratio of $\varphi = 0.8$. A comparable 50 kW flame at an equivalence ratio of $\varphi = 0.77$ and a pressure of 2 bara is shown in Fig. 5b. It can be seen that the increase in pressure serves to compact the overall flame as the flame front moves back towards the burner nozzle exit. This is most likely due to the drop in overall volumetric flow rate through the burner as well as changes in thermal and mass diffusion due to an increase in density, as the backpressure valve is closed.

Combustion testing in the HPGSB was then conducted on high-CO BOS gas-air flames at atmospheric pressure, 50 kW thermal power, and equivalence ratios from $0.49 < \varphi < 1.34$.

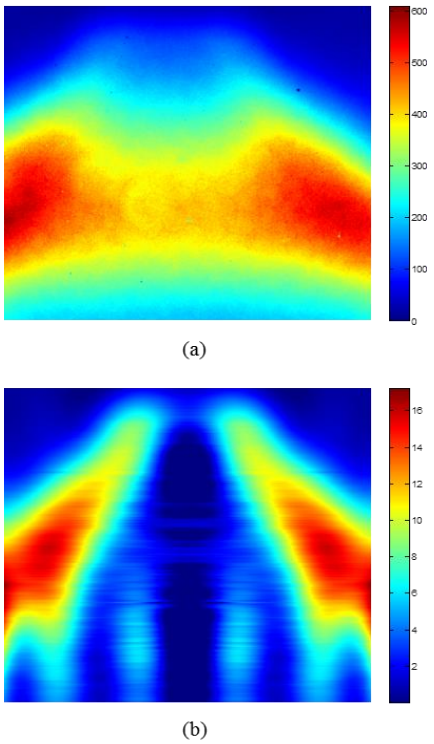

Fig. 4 Time-averaged OH* chemiluminescence image before (a) and after (b) Abel inversion for atmospheric BOS gas flame at 50 kW and φ = 1.0.

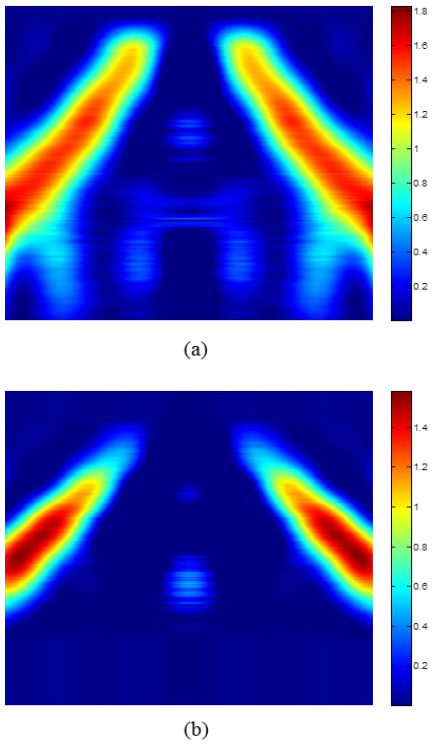

Fig. 5 Abel inversion of OH* chemiluminescence images for 50 kW CH_4-air flame at atmospheric pressure (a) and 2 bara (b).

Both OH* and CH* chemiluminescence measurements were taken at each test condition. Fig. 6 shows the CH* chemiluminescence image for the same 50kW BOS gas-air flame (φ = 0.98) as Fig.4 (OH* chemiluminescence). The image in Fig. 6a is only background corrected and time-averaged, whilst the image in Fig. 6b was the resulting spatially-resolved CH* chemiluminescence image after Abel inversion. Comparing Fig. 4a and Fig. 6a shows that there is a drop in signal intensity from OH* to CH* chemiluminescence, expected by the abundance of OH radicals in the reaction zone as compared to the expected concentration of CH radicals in the pre-reaction zone. Comparing further, the similarity in shape between Fig. 4 and Fig. 6 indicates that CO_2* chemiluminescence correction should be implemented, particularly for the CH* images, which, although showing potential CH radicals further upstream (note the shift of high intensity regions towards the burner nozzle exit), may be falsely including other active species chemiluminescence and ambient light (noted by the imperfections seen in the quartz confinement tube in Fig. 6a).

Finally, it has been shown [7,9,13] that the equivalence ratio can be correlated to the OH* and CH* chemiluminescence intensity for methane-air flames. As can be seen in Fig. 7, the OH* and CH* chemiluminescence intensity (calculated as integral intensity as in Fig. 3) peaks near stoichiometry (φ = 1), showing good agreement with trends identified in [7] and [9].

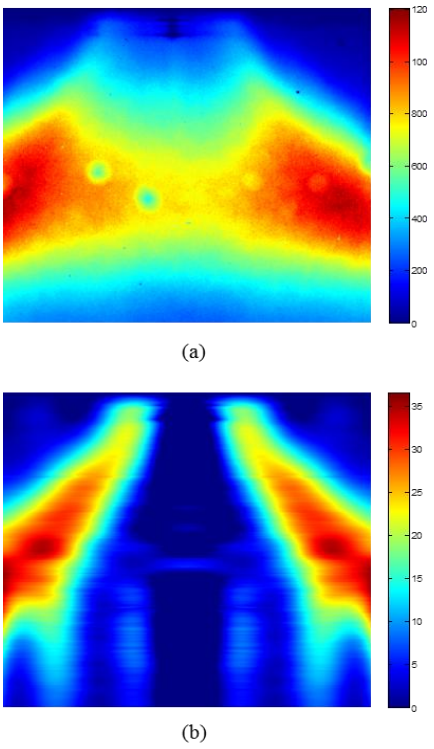

Fig. 6 Time-averaged CH* chemiluminescence image (a) and after Abel inversion (b) of atmospheric BOS gas flame at 50 kW and φ = 1.0.

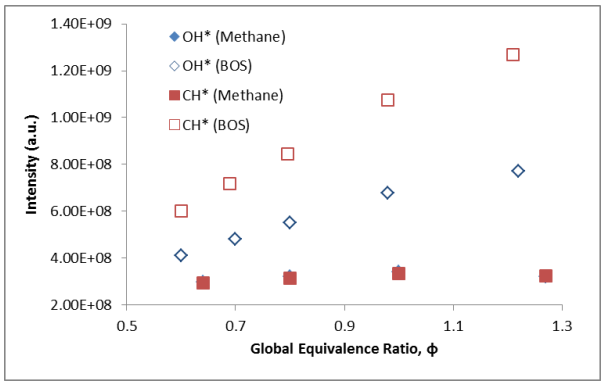

Fig.7 Effect of global equivalence ratio on the integral intensity of the measured OH* (diamond) and CH* (square) signal for both CH_4 and BOS gas.

However, it can be seen that the BOS gas flames do not exhibit the same behavior, with the intensity of both OH* and CH* chemiluminescence increasing well past $\varphi = 1$. This potentially suggests different reaction pathways resulting in the production of OH* and CH* chemiluminescence in high-CO syngas flames, and requires further investigation, particularly into the influence of broadband CO_2* chemiluminescence.

Conclusions

The development and commissioning of a chemiluminescence imaging system for the study of atmospheric and pressurised swirl flames at Cardiff University's GTRC has been completed through testing of both CH_4-air and BOS gas-air flames in the premixed HPGSB. Both OH* and CH* measurements were taken to demonstrate the following:

1) Validation of system equipment settings and image processing procedure, including background removal, temporal averaging, and deconvolution using an Abel inversion algorithm
2) The influence of equivalence ratio, pressure, and thermal power on chemiluminescence signal intensity
3) Comparison of chemiluminescence signal intensity between two fuels that differ greatly in composition

This installation sets the stage for future development of diagnostic capability at the GTRC, including planar laser induced fluorescence (PLIF) and advanced chemiluminescence techniques for enhanced temporal resolution of fundamental combustion phenomena, with a particular focus and interest in changes to flame structure resulting from thermoacoustic instabilities and fuel composition. Further study is also warranted into the production of OH and CH radicals in high-CO syngas flames for use as markers of flame stability and combustion efficiency.

Acknowledgements

This research outcome was funded through two projects, the Low Carbon Research Institute's (LCRI) Large-Scale Power Generation (LSPG) group, with funding provided from the Higher Education Funding Council for Wales (HEFCW) and the Flex-E-Plant Consortium, with funding provided through the UK Engineering and Physical Sciences Research Council (EPSRC). All experimental work was conducted at Cardiff University's Gas Turbine Research Centre in Margam, Wales, United Kingdom.

References

[1] P. Kutne, I. Boxx, M. Stöhr, W. Meier, Proc. Eur. Combust. Meet., 2005.
[2] G. Cabot, D. Vauchelles, B. Taupin, A. Boukhalfa, Exp. Therm. Fluid Sci. 28 (2004) 683-690.
[3] L.C. Haber, U. Vandsburger, W.R. Saunders, V.K. Khanna, An Experimental Examination of the Relationship between Chemiluminescence Light Emissions and Heat-release Rate Under Non-Adiabatic Conditions, Report No. RTO-MP-051, U.S. Department of Defense, 2001.
[4] M. Lauer, T. Sattelmayer, Proc. Int. Symp. Appl. Laser Tech. Fluid Mech., 2008.
[5] Y. Hardalupas, C.S. Panoutsos, G. Skevis, A.M.K.P. Taylor, Proc. Eur. Combust. Meet., 2005.
[6] H. P. Broida, A.G. Gaydon, Proc. R. Soc. Lond. A 218 (1953) 60-69.
[7] C.S. Panoutsos, Y. Hardalupas, A.M.K.P. Taylor, Combust. Flame 156 (2009) 273-291.
[8] V. Nori, J. Seitzman, AIAA-2008-953, 2008.
[9] D. Guyot, F. Guethe, B. Schuermans, A. Lacarelle, C.O. Paschereit, Proc. ASME Turbo Expo, Glasgow, 2010.
[10] A. Lantz, R. Collin, M. Aldén, A. Lindholm, J. Larfeldt, D. Lörstad, J. Eng. Gas Turbine Power 137 (2015) 031505-1-031505-8.
[11] R. Sadanandan, P. Kutne, A. Steinberg, W. Meier, Flow Turbul. Combust. 89 (2012) 275-294.
[12] B. Higgins, M.Q. McQuay, F. Lacas, J.C. Rolon, N. Darabiha, S. Candel, Fuel 80 (2001) 67-74.
[13] S. De Iuliis, D. Giassi, S. Maffi, F. Cozzi, R. Dondè, 35th Meet. Ital. Sect. Comb. Inst., Milan, 2012.
[14] U. Stopper, M. Aigner, W. Meier, R. Sadanandan, M. Stöhr, I. S. Kim, J. Eng. Gas Turbine Power 131 (2009) 021504-1-021504-8.
[15] M. Lauer, M. Zellhuber, T. Sattelmayer, C. Aul, J. Eng. Gas Turbine Power 133 (2011) 121501-1-121501-8.
[16] P. Kutne, B. Kapadia, W. Meier, M. Aigner, Proc. Combust. Inst. 33 (2011) 3383-3390.
[17] C. Killer, Abel Inversion Algorithm, MATLAB Central File Exchange, http://www.mathworks.com/matlabcentral/fileexchange/43639-abel-inversion-algorithm , 2014.
[18] G. Pretzler, Z. Naturforsch 46a (1991) 639-641.